Evaluation of Cardiovascular Stents as Antennas for Implantable Wireless Applications

Eric Y. Chow, *Student Member, IEEE*, Yuehui Ouyang, *Member, IEEE*, Brooke Beier, *Student Member, IEEE*, William J. Chappell, *Member, IEEE*, and Pedro P. Irazoqui, *Member, IEEE*

***Abstract*—In this study, we explore the use of stents as radiating structures to support transcutaneous wireless telemetry for data transfer of internal measurements from within the circulatory system. The implant location is chosen for the specific application of heart failure detection by monitoring internal pressure measurements of the pulmonary artery. The radiative properties of the single stent are quantified in free space within an anechoic chamber and compared with measurements taken while implanted in a live porcine subject. The *in vivo* studies of our 2.4-GHz stent-based transmitter, implanted at a depth of 3.5 cm within the chest, showed a 32–35-dB power reduction at a receive distance of 10 cm for both co- and cross-polarizations. The approximate far-field H-plane antenna pattern is quantified at a distance of 50 cm both in free space within an anechoic chamber and while implanted within a porcine chest. These results are used to explore the accuracy of a high-fidelity simulation model developed using Ansoft's High Frequency Structural Simulator and components of their Human Body Model to provide a model that is validated with empirical data. This study provides insight into the effects of tissue on high-frequency electromagnetic transcutaneous transmission and develops a high-fidelity model that can be used for further design and optimization.**

***Index Terms*—Biomedical applications of electromagnetic (EM) radiation, biomedical monitoring, biomedical telemetry, implantable biomedical devices.**

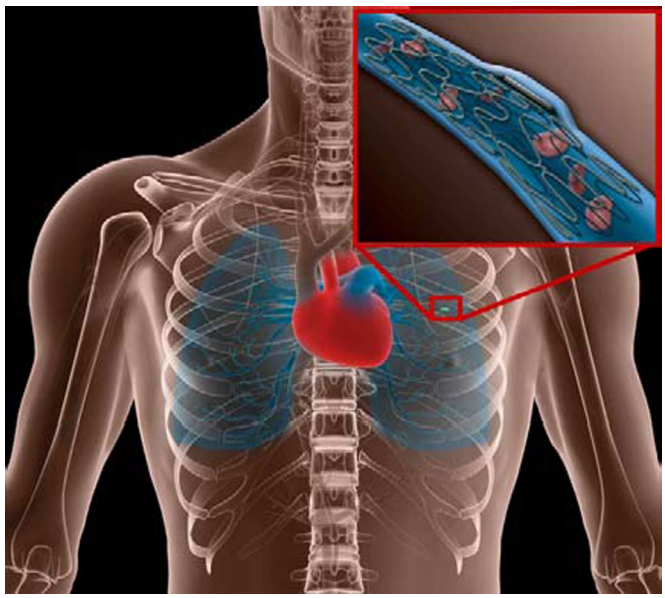

Fig. 1. Conceptual drawing of stent-based platform for implantable electronics implanted in a branch of the pulmonary artery.

I. Introduction

HEART failure affects approximately 2% of the adult population in developed countries and 6%–10% of people over the age of 65 [1]–[5]. During the first year after diagnosis, mortality rates of 30%–40% have been published, and after five years, this percentage increases to 60%–70% [5]–[7]. The burden imposed by advanced heart failure is compounded by frequent hospitalizations due to congestive or low-output symptoms, renal and respiratory dysfunction, anemia, arrhythmia, and other systemic complications.

A stent-based monitoring device implanted in the pulmonary artery, as shown in Fig. 1, can be used to provide internal measurements of pulmonary diastolic pressure, as well as other measures of cardiac health such as oxygenation, flow, and blood chemistry. It is generally accepted that pulmonary wedge pressure, together with cardiac output data, is the single most useful parameter for diagnosing and characterizing heart failure [8]. Pulmonary wedge pressure can be obtained from the pulmonary diastolic pressure because the difference between the two is small and generally fixed for each patient [9]. Catheterization of the right heart is routinely used in coronary and intensive care units to obtain the pulmonary pressures and cardiac output data in patients with severe heart failure and other complex heart diseases [10], [11]. Application of the technique to diagnose and guide treatment of heart failure patients at the bedside has been very limited due to the invasive nature of the technique and lack of a portable pulmonary pressure monitoring device [12].

This paper focuses on the evaluation of a stent-based antenna used to form a wireless data-link between an implant deep within the chest and the external environment. This novel prototype cardiac sensing platform utilizes a stent-based package that can be implanted with a simple minimally invasive outpatient procedure that does not occlude or obstruct blood flow after implantation. Integration of a miniature cardiac sensor and wireless transmitter with a Food and Drug Administration (FDA) approved medical

Manuscript received January 31, 2009; revised June 23, 2009. First published September 18, 2009; current version published October 14, 2009. This work was supported in part by SOLX Inc.

E. Y. Chow is with the Brain Computer Interface Laboratory, Weldon School of Biomedical Engineering, School of Electrical and Computer Engineering, Purdue University, West Lafayette, IN 47907 USA (e-mail: eychow@purdue.edu).

Y. Ouyang and W. J. Chappell are with the IDEAS Microwave Laboratory, School of Electrical and Computer Engineering, Purdue University, West Lafayette, IN 47907 USA (e-mail: ouyangy@purdue.edu; chappell@purdue.edu).

B. Beier and P. P. Irazoqui are with the Brain Computer Interface Laboratory, Weldon School of Biomedical Engineering, Purdue University, West Lafayette, IN 47907 USA (e-mail: bbeier@purdue.edu, pip@purdue.edu).

Color versions of one or more of the figures in this paper are available online at http://ieeexplore.ieee.org.

Digital Object Identifier 10.1109/TMTT.2009.2029954

stent, which acts as both the package substrate and radiating structure is introduced in [13] and [14]. The concept of using a stent to form a wireless link is shown by Takahata *et al.* in [15], where an antenna is carefully micromachined. This antenna has a similar form factor to a stent and is designed to allow for balloon deployment methods. The benefit of a stent or stent-like device is that it provides efficient data transfer from a device that can be implanted in nearly any vessel or body conduit. From the pulmonary artery, this device can take direct measurements of pulmonary diastolic pressure allowing for early diagnosis of heart failure [8].

A variety of implantable antennas have been explored in recent literature for numerous medical applications [16]–[18]. Spiral serpentine microstrip antennas are explored in [19] on a shoulder model derived from the University of Utah man model [20] and in [21] on skin mimicking gels. A planar inverted F-antenna integrated with an artificial pacemaker is measured in a muscle equivalent phantom in [22]. The "stentenna" developed in [15] and [23] is carefully micromachined to create a helical-like coil used as an inductor in an *LC* tank that can be passively interrogated. Testing of this stent-like antenna is done in air and a nonconductive liquid [23]. Although implantable antennas have been used extensively in biomedical devices, little work has been done to characterize their performance *in vivo* [24]–[27].

An active system is targeted in this study to allow for the transmission of amplified, filtered, and digitized data, which improves signal integrity and reduces noise immunity. Active implants also allow for the ability to individually address multiple implants and store data into on-chip memory. Current passive devices offer a simple and robust solution, but suffer from relatively poor signal-to-noise ratio, vulnerability to patient misuse, and limited functionality [28]–[30]. Active cardiac pressure monitors have been explored by companies and research groups, but are currently rather large due to components including a relatively large battery, which prevents the ability for placement directly into the pulmonary artery [31]–[33].

In this study, we quantify the radiative capabilities of commercially available stents, provided by Cook Medical, Bloomington, IN, through simulations and *in vivo* studies. We also develop a simulation model which integrates components from Ansoft Corporation's "Human Body Model" along with additional tissue types and layers allowing for evaluation of the electromagnetic (EM) effects of implantation. The *in vivo* data is compared with the simulation model to validate the accuracy of the model. This study aims toward developing and validating an accurate simulation model that can be used, as a substitute for costly *in vivo* trials, in further iterative design optimizations.

II. Design and Assembly

To validate the use of stents for this application, we examined a range of stent designs and settled on two popular mechanical structures corresponding to two different common delivery mechanisms. The first is the Formula 418 Balloon-Expandable Biliary Stent, and the second is a Zilver 635 Vascular Self-Expanding Stent, both provided by Cook Medical. Transmitter prototypes are assembled by integrating these two stent types with MAXIM Integrated Products voltage-controlled oscillators. The stents are first expanded to their final implantation size of 30 mm in length and 5–6 mm in diameter, shown in Fig. 2(a), using balloon catheters for the Formula 418 Balloon-Expandable Biliary Stents and a removable sleeve for the Zilver 635 Vascular Self-Expanding Stents. The stents are then integrated with a −3-dBm output, 2.4-GHz voltage-controlled oscillator (MAX2750) onto an FR-4 substrate along with external wires for supplying power. The integrated circuit (IC), traces, and exposed sections of wire are covered with a silicone sealant, while the stents themselves are left bare and are in direct contact with the tissue during and after implantation. External wires are used instead of a battery to ensure a reliable power supply to the transmitter, as well as to avoid the effects of having a large conductive object in the vicinity of the stent-based antenna. A section of anechoic wedge foam is used to cover the wires in order to help minimize their radiation. A grounding shield for the wires was not used because this implementation would present an unrepresentative large ground for the antenna and potentially enlarge the path through the incision site. The external powering wires still affect the measurement results of the stent-based antenna. These effects are studied through High Frequency Structure Simulator (HFSS) simulation comparisons of the stent-based antenna with and without wires. The simulations explored wire lengths varying from 0 to 50 cm and two

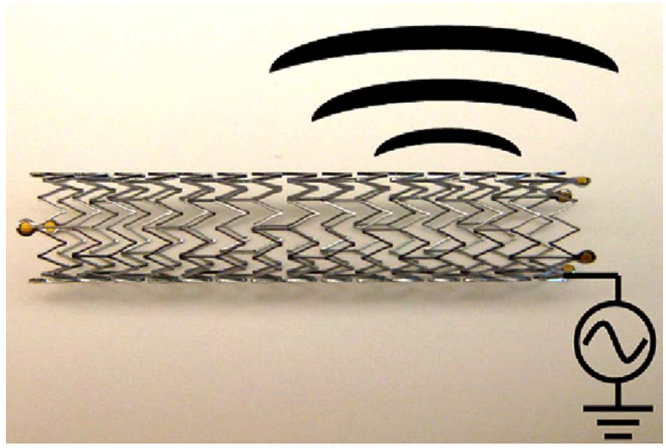

(a)

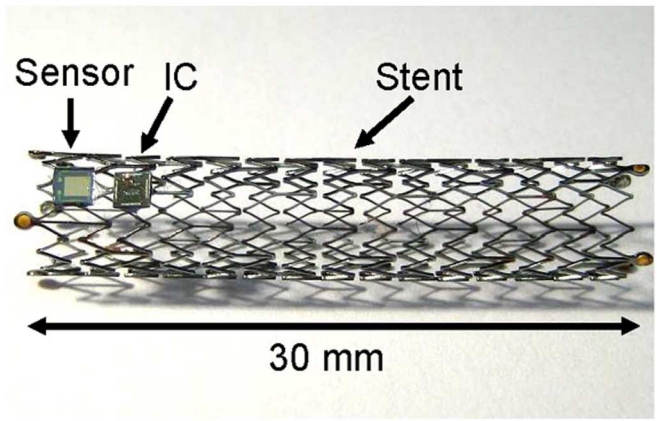

(b)

Fig. 2. (a) Zilver 635 Vascular Self-Expanding Stent arranged in a monopole-like configuration. (b) Conceptual nonfunctional prototype integrated with a MEMS capacitive sensor a application-specific integrated circuit (ASIC) with onboard transmitter, wireless powering, and sensor interface circuits.

wire orientations, parallel and perpendicular to the stent. For the range of wire lengths, the worst case results still show a relatively small gain variation of −2.8 to 2.3 dB for the parallel wire and −3.6 to 1.8 dB for the perpendicular wire.

The wires and printed circuit board (PCB) are used only for prototyping and the final device, as shown in Fig. 2(b), will have a wireless powering scheme with neither wires, nor a PCB. This scheme will also use the stent as the antenna to receive an upper megahertz to gigahertz frequency EM powering wave. Remote powering via EM propagation offers significant advantages over inductive powering techniques commonly seen in biomedical applications [34]. Inductive power requires precise alignment and relatively close distances between the external and implanted coils to achieve usable efficiencies [35]. RF powering utilizing EM propagation results in more orientation immunity and greater operating distances, which is desirable for use in a clinical environment [36]. As demonstrated in [36]–[39], the high-frequency power received by the antenna can be fed through an RF rectifier to generate the dc supply for the rest of the system. Although 2.4 GHz is chosen for data transfer, a lower frequency is likely desired for wireless powering to reduce the tissue absorption, which increases the efficiency of the power transfer and reduces the specific absorption rate (SAR) of the body. The IEEE C95.1 standard specified by the International Commission on Non-Ionizing Radiation Protection (ICNIRP) states that for frequencies between 10 MHz–10 GHz, the 6-min average SAR must be below 0.08 W/kg [40]. A lower frequency results in a lower absorption factor allowing for an increase in wireless power while maintaining a SAR that meets the guidelines.

The assembled prototype devices, with an expanded stent and voltage-controlled oscillator, measure 35 mm in length and 5–6 mm in diameter. The prototypes are sufficient for evaluating the amount of signal loss from transmission through the body, as well as the EM feasibility of our stent-based wireless sensing platform.

Higher microwave frequencies are advantageous due to the size constraints of the implant resulting in a miniature antenna, as well as the higher bandwidth availability [41]. The choice of operating frequencies is limited to the available bands allocated by the Federal Communications Committee (FCC), and therefore, precise optimization of operation frequency is unnecessary due to the large discretization of the available options. Bands of interest include the industrial, scientific, and medical (ISM) bands at 900 MHz, 2.4 GHz, and 5.8 GHz and the medical implant communications service (MICS) band at 400 MHz [42], [43]. An operating frequency is chosen by a comparison of the tissue- induced power loss (PL) with the efficiency of the stent radiator.

As a first-order approximation of the transcutaneous effects, a derivation of the attenuation of a wave through homogeneous muscle is performed [44]. The skin depth as a function of frequency and tissue dielectric properties is derived from the wave equation as

$$\delta(f) = \frac{1}{2\pi f\sqrt{\mu\varepsilon}\sqrt{\frac{1}{2}\left(\sqrt{1+\left(\frac{\sigma}{\omega\varepsilon}\right)^2}-1\right)}} \tag{1}$$

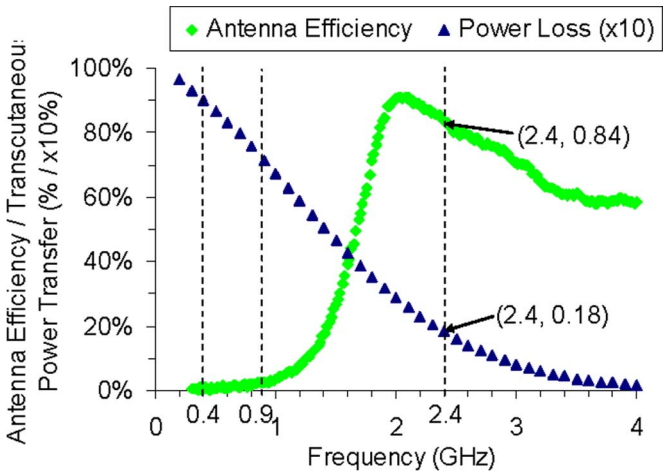

Fig. 3. Plot showing the calculated percentage of power transfer through 3.5 cm of muscle and antenna efficiency of the stents accounting for radiation and impedance mismatch efficiencies. Note that the PL percentage values are multiplied by a factor of ten in order to visualize the trend when plotted alongside the antenna efficiencies. Vertical dashed lines are placed at the 900-MHz and 2.4-GHz ISM bands and 400-MHz MICS band.

which is then used to calculate the power attenuation factor (AF) given by

$$\mathrm{AF} = e^{-z/\delta(f)}. \tag{2}$$

This calculation will only account for the EM absorption of the tissue and does not account for the multiple dielectric boundaries that the propagating wave will encounter. To evaluate the boundary conditions, we first consider a single tissue–air interface and calculate the reflection and transmission components at the interface. Since the tissue wave impedance is significantly less than that of the air, the transmission wave power will be reduced from that of the incident wave. The effect of the boundary conditions is calculated from a ratio of transmission power to incident power. Combining the boundary condition effects with the AF results in an overall PL factor given by

$$\mathrm{PL} = \frac{4\eta_{\mathrm{air}}\eta_{\mathrm{muscle}}}{(\eta_{\mathrm{air}}+\eta_{\mathrm{muscle}})^2}e^{-2z/\delta(f)}. \tag{3}$$

Using the dielectric properties of human muscle at 2.4 GHz measured in [45]–[47], the single interface results in a 60% reduction in power. The overall PL incorporating the absorption of a 3.5-cm tissue section calculated from the attenuation coefficient, results in a 98% (17.42 dB) reduction in power. This simplified loss calculation only accounts for a single interface and neglects transmission through heterogeneous media and multiple boundary conditions, but provides an approximation of the PL trends for the coarse optimization needed to select the band of operation. Previously published dielectric properties of human muscle are used to calculate the tissue-induced power attenuation due to a 3.5-cm section of muscle for various frequencies from 100 MHz to 7 GHz, which is plotted in Fig. 3 [45]–[47]. Note that the plot of this percentage is multiplied by a factor of ten in order to visualize the trend when plotted alongside the antenna efficiency.

It is well known that electrically large antennas will radiate more efficiently [48]. Stents provide the availability of a large

structure inside of the body, which does not obstruct blood flow or interfere with other bodily functions, and therefore, is a natural choice as a radiator. Unfortunately, the complex metal pattern of the stent increases the difficulty of the analysis, making the structure distinct from traditional analytical expressions for wire antennas requiring some laboratory measurements to supplement calculations. The impedance mismatch factor of the stent as a radiator is determined by measuring the reflection coefficient with a network analyzer [48]. The stent is assembled as an antenna above a well-defined ground plane to isolate the stray fields from the measurement cables. The connection to the stent is fed through the ground plane and then attached using a subminiature A (SMA) cable to port 1 of a network analyzer, which is then used to measure the reflection coefficient across frequencies. The bandwidth of the stent-based antenna, determined from this measured reflection coefficient, is 555 MHz. Radiation efficiency of our stent-based antenna is then calculated across frequencies using Wheeler and Chu's efficiency formulas [49]–[51]. The product of the impedance mismatch factor and the radiation efficiency provides the overall efficiency of the stent-based antenna, which is plotted versus frequency in Fig. 3 [48]. Out of the available frequency bands for biomedical applications, 2.4 GHz provides an optimal solution after considering the tradeoffs between the PL through the tissue and the desire for a relatively efficient antenna, and is the chosen operating frequency used throughout this study.

III. High-Frequency Simulation Models of Implanted Stent-Based Antennas

Simulation models are used to gain a better understanding of the surrounding biological environment and its effect on the radiating abilities of the stent, and provide a means for design and optimization of the wireless link. This study explores the actual level of modeling required to provide a reasonably accurate representation of an *in vivo* environment. The entire Ansoft human body model, which consists of a tremendous amount of different tissues and geometrical details, may not be necessary or even accurate. The high complexity of the model requires long simulation times and results in questionable convergence and accuracy.

In this study, we develop a simplified version of the whole body model by focusing on the upper chest region and isolating major biological features while later providing comparisons with measurements from *in vivo* studies. The simplified model, shown in Fig. 4(a), incorporates the lungs, parts of the respiratory tract, heart, and major veins and arteries from Ansoft's Human Body Model. The organs and other biological models consist of measured frequency-dependent tissue properties [45]–[47]. A custom three-layer tissue model is used to represent the remaining chest volume and takes on a cylindrical shape with a minimum radius of 130 mm, a maximum radius of 170 mm, and a height of 200 mm, which closely approximates the size of a human torso region [52]. In a human, the thicknesses of skin, fat, and muscle vary with location; however, we chose to implement a uniform elliptical model for the layers to provide a location-independent approximation of the implant's environment. The outermost layer of the cylindrical model is a 1-mm-thick layer of skin followed by a 3-mm section of fat, which models the epidermis, dermis, and subcutaneous tissue layers [53], [54]. The skin, fat, and muscle layers are set to the appropriate dielectric properties found in [45]–[47].

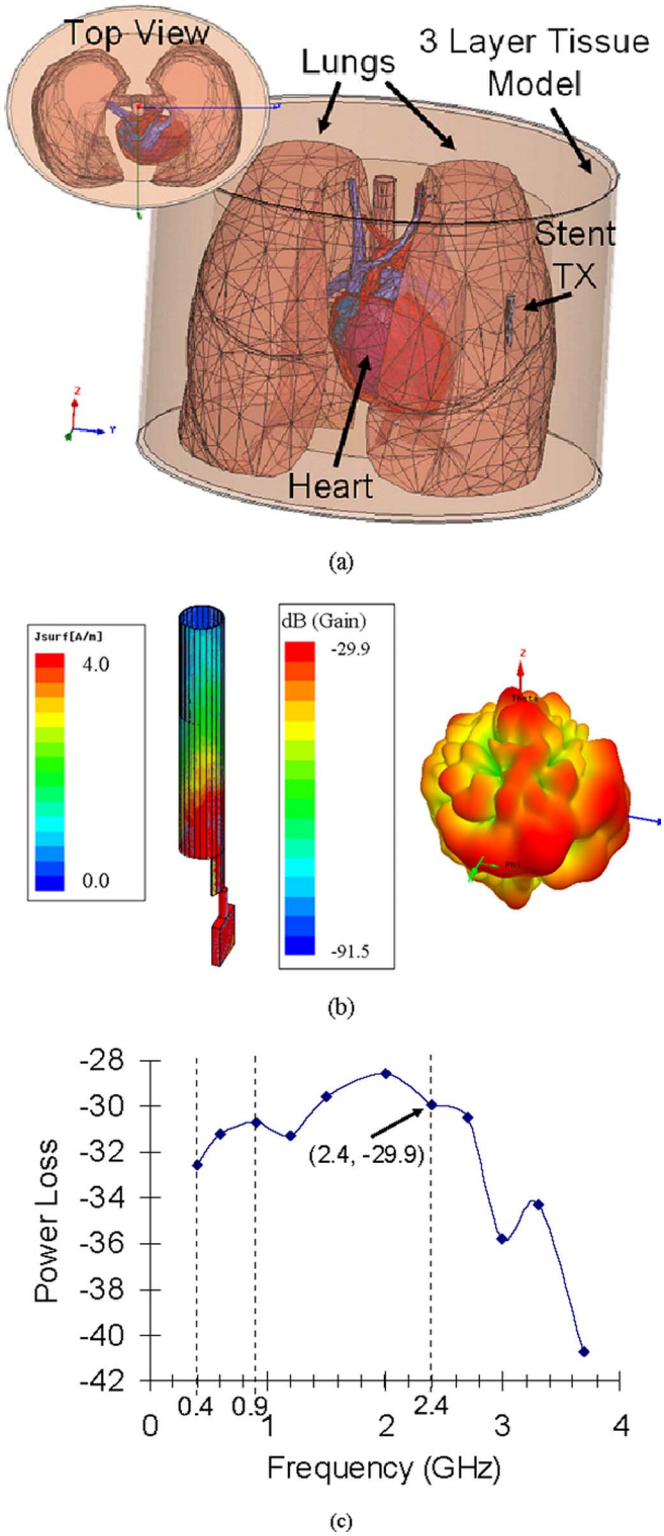

Fig. 4. (a) Model of the chest incorporating organs, major vessels, and other biological tissue types from Ansoft's Human Body Model along with a custom three-layer cylindrical tissue section. The stent-based transmitter is positioned in the lung representing the location of a pulmonary arterial branch. (b) Simulated surface current of the stent-based transmitter its radiation pattern while implanted in the pulmonary arterial region in the chest model.

To model both the Formula 418 and Zilver 635 stents, a hollow stainless-steel cylinder is used with a length of 30 mm, a diameter of 5 mm, and a thickness of 150 μm. Since the fine structural features of an actual stent have sub-wavelength dimensions at 2.4 GHz, a simplified model is sufficient to characterize the radiation property of the stent-based antenna while significantly reducing simulation complexity and time. A voltage excitation is applied between the end of the stent antenna and a small conductive ground designated as the transmitter IC, as shown in Fig. 4(b). This ground plane is 5 mm $\times$ 5 mm in area and 1 mm in thickness and is used to model the ground reference of the voltage-controlled oscillator (MAX2750). The stent-based antenna in free space is simulated to have a realized gain of -1.8 dBi and an omnidirectional radiation pattern in the azimuth plane. Due to limitations imposed by assembly and the surgical technique, the designed stent-based antenna has an asymmetric structure when compared to a traditional dipole. Therefore, there is a lot of current crowding on the small ground plane, which reduces the achievable gain of the antenna.

The stent-based transmitter model is then integrated with our simplified human torso model to simulate the radiative properties of the device after implantation. The stent is placed in the left lung, which corresponds to the location of the pulmonary arterial branches, and positioned 3.5 cm from the surface of the chest. In an initial simulation, the stent is filled with an air dielectric and the resulting realized gain is -17.5 dB. The decibel difference between this implanted realized gain and the -1.8-dBi value in free space is -15.7 dB and represents the tissue-induced PL. This value is similar to the 17.42-dB loss calculated in the analytical analysis above with differences attributed to the simplifications of the mathematical model. The stent is then filled with a blood dielectric to represent the true clinical setting and the realized gain in this case is simulated to be -29.9 dB, which results in a 28.1-dB power reduction. The simulated realized gain radiation pattern is plotted in Fig. 4(b). Although the dielectric properties of the tissue used in this model represents empirical data, the simulation accuracy is still in question. In Sections IV–VI, this simulated PL will be validated with *in vivo* studies and the H-plane cross section of the simulated antenna pattern will be plotted in comparison with the measured data.

Simulation results of the total PL incorporating tissue effects, including absorption and boundary conditions, impedance mismatches, and antenna efficiency is shown in Fig. 4(c) as a function of frequency. The coarse analytical frequency optimization shown in Fig. 3 provides reasonably consistent results with the more detailed simulation. These simulation results also show 2.4 GHz as a reasonably optimal ISM band for this implantable application.

IV. Measurements and *In Vivo* Surgeries

The free-space performance of the stent-based transmitter prototypes are first characterized inside an anechoic chamber. An 8-dBi horn antenna is placed on a stand inside the anechoic chamber and fed through a 1.96-dB loss SMA cable that runs out of the chamber where it connects to a spectrum analyzer. The stent-based transmitter is placed on a stand directly in front of the horn antenna and the powering wires are connected to a power supply. The distance between the receive horn antenna and the stent-based transmitter is set to 10 cm, which is a rough approximation of the practical distance a clinician or patient would hold the external receiving device when data collection from the implant is desired. The received power for the device is then measured for both co- and cross-polarizations. The received powers at a free-space distance of 10 cm from both Formula 418 and Zilver 635 based transmitters are practically the same and a 9-dB power reduction is seen when the orientation is changed from co-polarization to cross-polarization.

Antenna pattern measurements are then taken by rotating the stent-based transmitter such that the stationary receive horn antenna is directed at different points on the H-plane of the stent. It should be noted that the powering wire is bent backwards a few inches under the stent, which affects this antenna pattern. The effect is more significant on measurements taken from the backside of the stent-based transmitter. Therefore, a roughly omnidirectional pattern is seen in the front side of the device, while the backside deviates from this ideal pattern. The results from these measurements are later used to compare with implanted data.

Motivated by the radiating ability of the prototype in simulations and free space, the potential clinical value of the stent-based platform is validated with *in vivo* studies to verify that the prototype is capable of forming a wireless link once implanted in the pulmonary artery of a living body. *In vivo* studies are performed on several American Yorkshire pigs ranging in weight from 35 to 40 kg. The surgical procedure follows the Institutional Animal Care and Use Committee (IACUC) approved protocol (No. 08–019). Anesthesia is induced with a combination of Telazol (250-mg tiletamine and 250-mg zolazepam), ketamine (250 xmg), and xylazine (250 mg) intramuscularly. Anesthesia is maintained with inhalation anesthetics composed of Isoflurane (1.5%–4.0% oxygen) administered from a machine with a vaporizer and waste gas ventilation system. Throughout the procedure, muscle tone, reflexes, respiration, temperature, electrocardiogram (ECG), and blood pressure are carefully monitored.

Although there are obvious geometrical differences between porcine and human species, there are enough similarities to justify the use of a swine for approximating a human. According to [46], there may actually be a greater variation of tissue properties between two humans than between porcine and human species. Pigs are often used for their anatomical similarities according to [55] and [56] and while geometrical differences exist, the swine still provides a reasonable approximation in terms of dimensions and size [57].

For *in vivo* studies, our surgical and experimental setup, shown in Fig. 5, consists of the porcine test subject, horn antenna, spectrum analyzer, and power supplies. The implantation of our device in the porcine chest cavity begins with an incision about 2 cm in length in the neck region of the swine. Trough a blunt dissection method, the inner tissue layers are then separated dorsally to a depth of 3.5 cm and caudally towards the rib cage. After reaching the rib cage, the prototype is inserted through the incision and placed just outside of the rib cage at a depth of 3.5 cm from the surface of the chest, as shown in the Fig. 6 radiograph. Once the device is implanted in the porcine

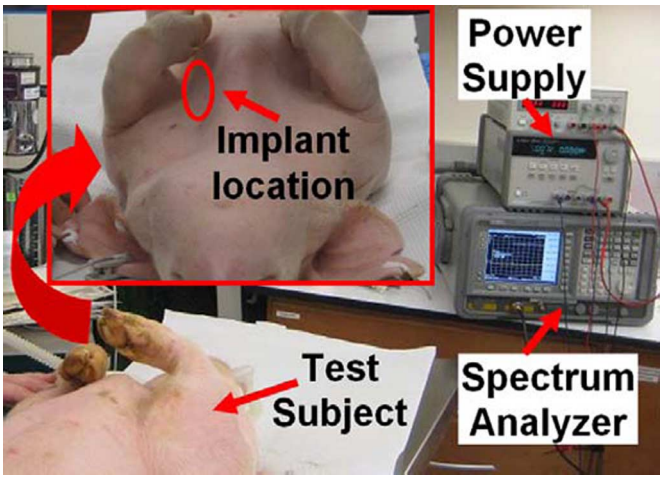

Fig. 5. Experimental setup showing the porcine test subject and implant location along with measurement equipment.

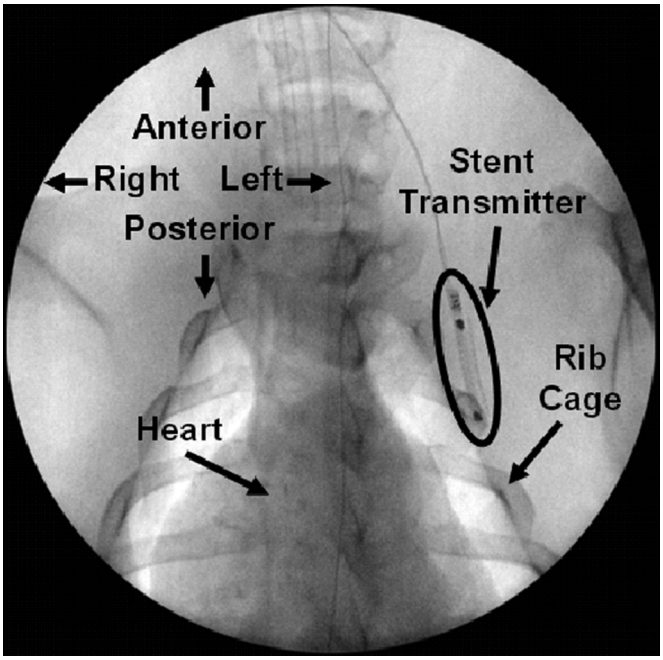

Fig. 6. Radiograph of *in vivo* study showing stent-based transmitter implanted 3.5 cm beneath the chest surface positioned in the upper left side of the porcine chest just outside of the rib cage.

chest, sutures are placed to close the muscle and skin layers over the implant. Anechoic wedge foam is used to cover the external powering wires. An 8-dBi horn antenna is then placed in front of (ventral to) the chest wall and fed into a spectrum analyzer to measure the power transmitted through the chest from the implant. A distance of 10 cm is chosen to provide an approximation of the practical distance a clinician or patient would hold the external receiving device when data collection from the implant is desired. Data is taken for both cross- and co-polarization. The antenna pattern in the H-plane for an implanted setting is also quantified over 180°, at 30° intervals, across the spinal cord axes on the ventral hemisphere of the porcine body. For a sufficiently thorough dataset, three porcine surgeries are performed, measurements are repeated numerous times, and multiple data sets are recorded and compared.

TABLE I
POWER RECEIVED FROM THE IMPLANTABLE STENT-BASED TRANSMITTER

Environment	Stent	Polarization	Received Power (dBm)[a]	Power Loss (dB)
Simulation	Formula 418 / Zilver 635	Co	--	28[b]
Free Space	Formula 418 / Zilver 635	Co	-27.142	--
Free Space	Formula 418 / Zilver 635	Cross	-35.788	--
Implanted	Formula 418	Co	-59.528	32.386
Implanted	Formula 418	Cross	-69.118	33.33
Implanted	Zilver 635	Co	-61.726	34.584
Implanted	Zilver 635	Cross	-67.32	31.532

[a]The power measurements are taken at a distance of 10 cm from the implantable device and the presented data subtracts out the gains of the 8 dBi horn antenna and 38 dB LNA while adding in the loss of the SMA cables.

[b]The simulated power loss is calculated by taking the dB difference between the realized gain while implanted and that in free space

V. RESULTS

The *in vivo* measurements, tabulated in Table I along with the free space and simulation results, validate the ability to wirelessly transmit out of the body from within the chest. The implanted transmitter has an output power of −3 dBm and the received power values are measured with the horn antenna positioned ventral to the chest at a distance of 10 cm from the implant. The Zilver 635 vascular self-expanding stent and Formula 418 balloon-expandable biliary stent had similar performance in both free space and an implanted setting. A comparison of polarizations shows a 6–10-dB reduction when changing from co- to cross-polarized. The PL due to the tissue is determined by comparing the implanted measurements with those done in free space within an anechoic chamber. The Formula 418 stent-based transmitter shows about 32.4–33.3 dB of PL after implantation. The Zilver 635 stent-based device shows about 31.5–34.6 dB of power reduction. The receive power at 10 cm for the different polarizations is tabulated in Table I. This transmit distance is representative of measurements done by a clinician near the chest of the patient. As the transmit distance is increased to 1 m, the data represents an approximate far-field pattern and the fall off beyond this point is described by Friis transmission equation [44]. The implanted co-polarized received power at 1 m for the Formula 418 and Zilver 635 stents are measured to be 74.3 and 76.8 dBm, respectively.

Antenna pattern measurements for the stent-based device across the H-plane are taken in both free space and implanted settings and are plotted alongside the simulation results in Fig. 7. An anechoic chamber is used for the free-space case and the radiation pattern is quantified across the H-plane. During the *in vivo* experiments, measurements are only taken across 180° around the ventral hemisphere of the porcine body because of difficulties in accessing the dorsal side of the swine due to restrictions imposed by the surgical environment. For the antenna pattern measurements, the receive antenna is positioned 50 cm from the implant to represent the far-field

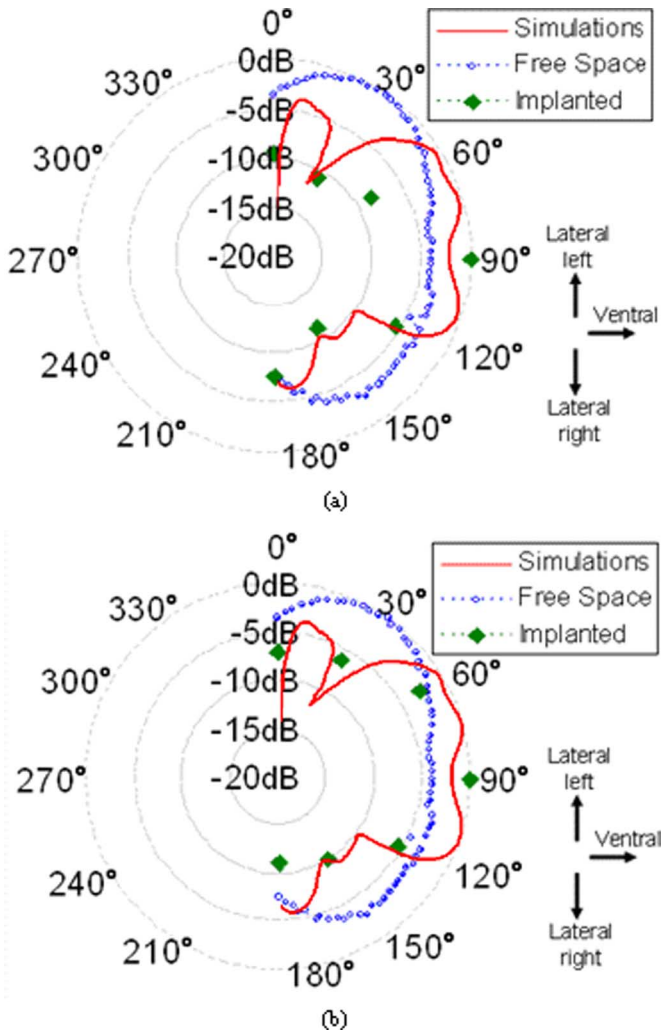

Fig. 7. Antenna patterns from simulations and measurements in free space and implanted settings of the stent-based transmitters with the: (a) Formula 418 biliary stent and (b) Zilver 635 self-expanding stent. Laterally left of the porcine body is designated as 0°, directly ventral to the chest wall is 90°, and laterally right is 180°.

antenna pattern. The received power data are recorded at 30° increments across the H-plane in the ventral hemisphere for both the Formula 418 and Zilver 635 stent-based implants and are shown in the polar plots of Fig. 7. Directly lateral to the left side of the porcine body is designated as 0°, ventral to the chest is 90°, and lateral to the right side is 180°. The plots show the receive power levels in decibels after being normalized to the maximum power, which is seen when the receive antenna is positioned directly ventral to the chest.

VI. Discussion

This measured PL, ranging from 31.5 to 34.6 dB, differs by a few decibels from the simulated results of 28 dB. The differences are attributed to multiple factors. As shown in simulation and measurements, the implanted stent-based antenna has ripples in its radiation pattern, and thus, the measured power received could be several decibels lower than the maximum power delivered to that location. The simulation environment will always capture the maximum gain, but in an experimental setting, the actual power transfer measured could be a few decibels lower. Another factor for the variation stems from the approximations of the simulation model. Although the model itself is detailed, it does not capture some of the aspects such as the porous structure of the lung and the rib cage. Furthermore, as explained above, there are slight morphological differences between a swine chest and that of a human. A third factor is the external wires used in the measurements which, as discussed above, is simulated to produce a −3.6–2.3-dB variation depending on wire placement and orientation. The feasibility of measuring the maximum power transfer, the simplifications of the simulation model, and the powering wires are factors that contribute to the several decibel differences between our model and measurements.

For both the *in vivo* measurements and in simulations, the gain decreases as we angle away from the 90° orientation. The resulting antenna pattern for both device types after implantation has a narrower main beam-width than the more omnidirectional-like pattern observed in free-space measurements taken in the anechoic chamber. This deviation is expected because as the receive antenna travels toward either side of the porcine body, the direct line-of-sight path of the implanted transmitter travels through greater overall tissue thicknesses, as well as additional tissue sections and layers. This maximum power reduction is about 10 dB for the various angles across the ventral hemisphere of porcine body. The measured antenna patterns are similar to those seen in simulations and the differences can be attributed to various effects including multipath, anatomical, and geometrical differences between porcine and human species and simulation approximations. The results also quantify the power transfer for two polarizations and various angles and show that a co-polarized orientation positioned directly ventral to the chest is the most optimal placement to maximize power transfer, and thus, signal reception. This information is valuable as it provides the optimal placement and orientation of the external receive antenna for the stent-based implant in a clinical setting.

The measured power received values of 74–77 dBm at a distance of 1 m can be picked up by an external receiver to form a wireless data link. The ZigBee standard, which targets low power, low data rate, and short-range telemetry applications similar to that of this study, specifies a −91-dBm minimum sensitivity [58], [59]. At a distance of 1 m, and implanted 3.5 cm in the chest of a live porcine subject, the −3-dBm transmitter provides well above the minimum detectable signal specified by the standard. As a result, future iterations of the transmitter can reduce the output power by about 15 dB, down to −18 dBm, to lower the overall power consumption of the implant. The power can be further reduced if a range of less than 1 m is required in the clinical setting.

Simulation results match up reasonably well with *in vivo* data predicting PL values to within a few decibels and producing relatively similar antenna patterns, which suggests that our level of modeling may be sufficient. The development of this representative model allows for future iterative designs. The characteristics of the stent itself, including dimensions, material, and placement, are set by clinical and surgical requirements, and thus, the optimization must come from impedance matching and transmitter design. The validated simulation model developed in this study provides a method for further fine-tuning and precise optimization.

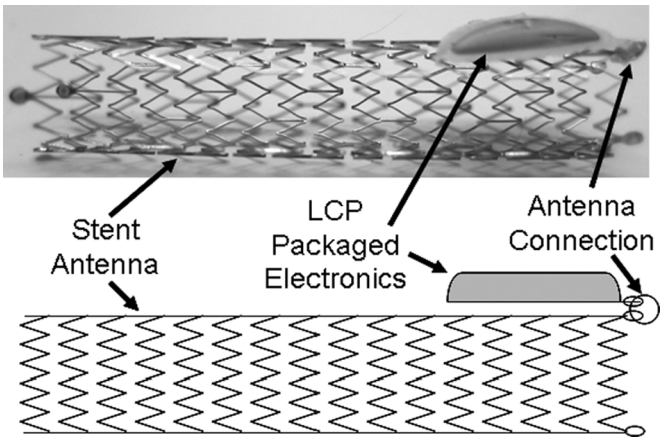

Fig. 8. Conceptual image and drawing of final LCP packaged system integrated with a stent. The antenna feed is achieved using a conductive ring that connects a ring on the LCP package with that on the stent.

The final packaging of the system will comprise of a liquid crystal polymer (LCP) material used to hermetically seal the electronics. The biocompatibility and chemical inertness of LCP is verified in [60]–[62] and its ability for micromachining makes this material promising as a substrate and package for the electronics. The hermeticity of LCP is also verified in [63] through ASTM-E 595-3 out-gassing tests and Method 1014, MIL-STD-883 gross leak and fine leak tests [64], [65]. A conceptual image and drawing of the final assembled system is shown in Fig. 8. The electronics are packaged in an LCP substrate consisting of the interconnects and antenna feed. Through a series of conductive rings, the antenna is fed out of the LCP package and connected to the stent.

The Formula 418 balloon-expandable and Zilver 635 self-expandable stents have comparable antenna performance; however, from a surgical perspective, the self-expandable stents are more desirable. Deployment of balloon-expandable stents requires relatively high pressures to ensure complete expansion. Self-expandable stents, composed of a nitinol shape memory alloy, achieves full expansion slowly after removal of a surrounding sleeve resulting in minimal stresses on the packaged electronics.

VII. Conclusion

This study has shown and quantified transcutaneous data and power transfer at 2.4 GHz from a stent-based transmitter implanted within the chest cavity through simulation models and *in vivo* studies. Two stent types, balloon expandable and self-expandable, are used to develop implantable transmitter prototypes whose technology may be used as a platform for internal cardiac monitoring. Furthermore, we develop a simulation model that integrates a custom three-layer cylindrical torso model with the primary organs in the chest and other biological features from Ansoft's Human Body Model. The efficacy of the simulations are evaluated and validated through *in vivo* measurements, which show that the model provides a reasonable prediction of the radiation pattern and tissue-induced PL that is accurate to within a few decibels.

Acknowledgment

The authors would like to thank Cook Medical, Bloomington, IN, for providing us with a variety of stents, catheters, and other medical supplies, Ansoft Corporation, Pittsburgh, PA, for providing us with their "Human Body Model," and our lab technician, C. Ellison, for his help in all the surgeries.

References

[1] M. Kupari, M. Lindroos, A. M. Iivanainen, J. Heikkil, and R. Tilvis, "Congestive heart failure in old age: Prevalence, mechanisms and 4-year prognosis in the Helsinki ageing study," *J. Int. Med.*, vol. 241, pp. 387–394, 1997.

[2] O. W. Nielsen, J. Hilden, C. T. Larsen, and J. F. Hansen, "Cross sectional study estimating prevalence of heart failure and left ventricular systolic dysfunction in community patients at risk," *Heart*, vol. 86, pp. 172–178, Aug. 2001.

[3] M. M. Redfield, S. J. Jacobsen, J. C. Burnett, Jr, D. W. Mahoney, K. R. Bailey, and R. J. Rodeheffer, "Burden of systolic and diastolic ventricular dysfunction in the community: Appreciating the scope of the heart failure epidemic," *J. Amer. Med. Assoc.*, vol. 289, pp. 194–202, Jan. 2003.

[4] A. Mosterd, A. W. Hoes, M. C. d. Bruyne, J. W. Deckers, D. T. Linker, A. Hofman, and D. E. Grobbee, "Prevalence of heart failure and left ventricular dysfunction in the general population: The Rotterdam study," *Eur. Heart J.*, vol. 20, pp. 447–455, Mar. 1999.

[5] K. K. Ho, J. L. Pinsky, W. B. Kannel, and D. Levy, "The epidemiology of heart failure: The Framingham study," *J. Amer. Coll. Cardiol.*, vol. 22, pp. 6A–13A, 1993.

[6] V. L. Roger, S. A. Weston, M. M. Redfield, J. P. Hellermann-Homan, J. Killian, B. P. Yawn, and S. J. Jacobsen, "Trends in heart failure incidence and survival in a community-based population," *J. Amer. Med. Assoc.*, vol. 292, pp. 344–350, Jul. 2004.

[7] M. R. Cowie, D. A. Wood, A. J. S. Coats, S. G. Thompson, V. Suresh, P. A. Poole-Wilson, and G. C. Sutton, "Survival of patients with a new diagnosis of heart failure: A population based study," *Heart*, vol. 83, pp. 505–510, May 2000.

[8] E. Topol, *Comprehensive Cardiovascular Medicine*. Philadelphia, PA: Lippincott-Raven, 1998.

[9] D. S. Baim and W. Grossman, *Grossman's Cardiac Catheterization, Angiography, and Intervention*, 6th ed. Philadelphia, PA: Lippincott, Williams, Wilkins, 2000.

[10] W. Forssmann, "Die sondierung des rechten herzens," *J. Molecular Med.*, vol. 8, pp. 2085–2087, 1929.

[11] A. Cournand, "Cardiac catheterization: Development of the technique, its contribution to experimental medicine and its initial application to man," *Acta. Med. Scand.*, vol. 579, pp. 3–32, 1975.

[12] H. Mueller *et al.*, "Present use of bedside right heart catheterization in patients with heart disease," *J. Amer. Coll. Cardiol.*, vol. 32, pp. 840–864, 1998.

[13] E. Y. Chow and P. P. Irazoqui, "Wireless implantable stent-based cardiac pressure sensor," presented at the BMES Annu. Fall Meeting, St. Louis, MO, Oct. 2–4, 2008.

[14] E. Y. Chow, B. Beier, Y. Ouyang, W. J. Chappell, and P. P. Irazoqui, "High frequency transcutaneous transmission using stents configured as a dipole radiator for cardiovascular implantable devices," presented at the IEEE MTT-S Int. Microw. Symp., Boston, MA, Jun. 7–12, 2009.

[15] K. Takahata, Y. B. Gianchandani, and K. D. Wise, "Micromachined antenna stents and cuffs for monitoring intraluminal pressure and flow," *J. Microelectromech. Syst.*, vol. 15, no. 5, pp. 1289–1298, Oct. 2006.

[16] E. Y. Chow, C.-L. Yang, A. Chlebowski, S. Moon, W. J. Chappell, and P. P. Irazoqui, "Implantable wireless telemetry boards for *in vivo* transocular transmission," *IEEE Trans. Microw. Theory Tech.*, vol. 56, no. 12, pp. 3200–3208, Dec. 2008.

[17] E. Y. Chow, C.-L. Yang, A. Chlebowski, W. J. Chappell, and P. P. Irazoqui, "Miniature antenna for RF telemetry through ocular tissue," in *IEEE MTT-S Int. Microw. Symp. Dig.*, 2008, pp. 1309–1312.

[18] E. Y. Chow and A. K. P. Irazoqui, "High data-rate 6.7 GHz wireless ASIC transmitter for neural prostheses," in *29th Annu. Int. IEEE Med. Biol. Soc. Conf.* , 2007, pp. 6580–6583.

[19] P. Soontornpipit, C. M. Furse, and C. Y. Chung, "Design of implantable microstrip antenna for communication with medical implants," *IEEE Trans. Microw. Theory Tech.*, vol. 52, no. 8, pp. 1944–1951, Aug. 2004.

[20] O. P. Gandhi and C. M. Furse, "Millimeter-resolution MRI-based models of the human body for electromagnetic dosimetry from ELF to microwave frequency," in *Proc. Int. Radiol. Protection Board Workshop*, Chilton, U.K., Jul. 1995, pp. 24–31.
[21] T. Karacolak, A. Z. Hood, and E. Topsakal, "Design of a dual-band implantable antenna and development of skin mimicking gels for continuous glucose monitoring," *IEEE Trans. Microw. Theory Tech.*, vol. 56, no. 4, pp. 1001–1008, Apr. 2008.
[22] T. Houzen, M. Takahashi, K. Saito, and K. Ito, "Implanted planar inverted F-antenna for cardiac pacemaker system," in *Int. Antenna Technol. Workshop*, Nov. 2008, pp. 346–349.
[23] K. Takahata, A. DeHennis, K. D. Wise, and Y. B. Gianchandani, "Stentenna: A micromachined antenna stent for wireless monitoring of implantable microsensors," in *Proc. IEEE 25th Annu. Int. Eng. Med. Biol. Soc. Conf.*, 2003, vol. 4, pp. 3360–3363.
[24] T. Akin, K. Najafi, and R. M. Bradley, "A wireless implantable multichannel digital neural recording system for a micromachined sieve electrode," *IEEE J. Solid-State Circuits*, vol. 33, no. 1, pp. 109–118, Jan. 1998.
[25] K. D. Wise, D. J. Anderson, J. F. Hetke, D. R. Kipke, and K. Najafi, "Wireless implantable microsystems: High-density electronic interfaces to the nervous system," *Proc. IEEE*, vol. 92, no. 1, pp. 76–97, Jan. 2004.
[26] R. R. Harrison, P. T. Watkins, R. J. Kier, R. O. Lovejoy, D. J. Black, B. Greger, and F. Solzbacher, "A low-power integrated circuit for a wireless 100-electrode neural recording system," *IEEE J. Solid-State Circuits*, vol. 42, no. 1, pp. 123–133, Jan. 2007.
[27] E. Y. Chow, B. Beier, W. J. Chappell, and P. P. Irazoqui, "Towards an implantable wireless cardiac monitoring platform integrated with an FDA approved cardiovascular stent," *J. Interventional Cardiol.*, vol. 22, Oct. 2009.
[28] M. Fonseca, M. Allen, D. Stern, J. White, and J. Kroh, *Implantable Wireless Sensor for Pressure Measurement Within the Heart*, A61B005/0215 U.S. ed. Atlanta, GA: CardioMEMS Inc., 2005.
[29] M. Allen *et al., Implantable Wireless Sensor for Blood Pressure Measurement With an Artery*. Atlanta, GA: CardioMEMS Inc., 2005.
[30] J. Joy *et al., Communicating With Implanted Wireless Sensor*. Atlanta, GA: CardioMEMS Inc., 2007.
[31] T. Bennett *et al.*, "Development of implantable devices for continuous ambulatory monitoring of central hemodynamic values in heart failure patients," *Pacing Clin. Electrophys.*, vol. 28, pp. 573–584, 2005.
[32] N. Najafi and C. A. Rich, *Method for Monitoring a Physiologic Parameter of Patients With Congestive Heart Failure*. Ypsilanti, MI: Integ. Sens. Syst. Inc., 2006.
[33] N. Najafi and A. Ludomirsky, "Initial animal studies of a wireless, batteryless, MEMS implant for cardiovascular applications," *Biomed. Microdevices*, vol. 6, pp. 61–65, 2004.
[34] K. V. Schuylenbergh and R. Puers, "Self-tuning inductive powering for implantable telemetric monitoring systems," *Sensors Actuators A, Phys.*, vol. 52, pp. 1–7, 1996/4//.
[35] M. Soma, D. C. Galbraith, and R. L. White, "Radio-frequency coils in implantable devices: Misalignment analysis and design procedure," *IEEE Trans. Biomed. Eng.*, vol. BME-34, no. 4, pp. 276–282, Apr. 1987.
[36] F. Kocer and M. P. Flynn, "A new transponder architecture with on-chip ADC for long-range telemetry applications," *IEEE J. Solid-State Circuits*, vol. 41, no. 5, pp. 1142–1148, May 2006.
[37] M. Changming, Z. Chun, and W. Zhihua, "A low-power AC/DC rectifier for passive UHF RFID transponders," in *Int. Microw., Antennas, Propag., EMC Technol. Wireless Commun. Symp.*, 2007, pp. 309–314.
[38] F. Alessio and A. Boni, "A CMOS analog frontend for a passive UHF RFID tag," in *Proc. Int. Low-Power Electron. Design Symp.*, 2006, pp. 280–285.
[39] K. Seemann, G. Hofer, F. Cilek, and R. Weigel, "Single-ended ultra-low-power multistage rectifiers for passive RFID tags at UHF and microwave frequencies," in *IEEE Radio Wireless Symp.*, 2006, pp. 479–482.
[40] ICNIRP, "Guidelines for limiting exposure to time-varying electric, magnetic, and electromagnetic fields (up to 300 GHz)," *Health Phys.*, vol. 74, pp. 494–522, 1998.
[41] G. C. Crumley, N. E. Evans, J. B. Burns, and T. G. Trouton, "On the design and assessment of a 2.45 GHz radio telecommand system for remote patient monitoring," *Med. Eng. Phys.*, vol. 20, pp. 750–755, 1999.
[42] *Title 47 of the Code of Federal Regulations Part 18—Industrial, Scientific, and Medical Equipment*. Washington, DC: FCC, 2007, vol. 1, pp. 878–878.
[43] *Title 47 of the Code of Federal Regulations Part 95—Personal Radio Services*. Washington, DC: FCC, 2007, vol. 5, pp. 553–554.
[44] C. A. Balanis, *Advanced Engineering Electromagnetics*. New York: Wiley, 1989.
[45] C. Gabriel, S. Gabriel, and E. Corthout, "The dielectric properties of biological tissues: I. Literature survey," *Phys. Med. Biol.*, vol. 41, pp. 2231–2249, 1996.
[46] S. Gabriel, R. W. Lau, and C. Gabriel, "The dielectric properties of biological tissues: II. Measurements in the frequency range 10 Hz to 20 GHz," *Phys. Med. Biol.*, vol. 41, pp. 2251–2269, 1996.
[47] S. Gabriel, R. W. Lau, and C. Gabriel, "The dielectric properties of biological tissues: III. Parametric models for the dielectric spectrum of tissues," *Phys. Med. Biol.*, vol. 41, pp. 2271–2293, 1996.
[48] D. M. Pozar, *Microwave and RF Design of Wireless Systems*, 1st ed. New York: Wiley, 2000.
[49] L. J. Chu, "Physical limitations of omni-directional antennas," *J. Appl. Phys.*, vol. 19, pp. 1163–1175, 1948.
[50] H. A. Wheeler, "Fundamental limitations of small antennas," *Proc. IRE*, vol. 35, no. 12, pp. 1479–1484, Dec. 1947.
[51] H. Wheeler, "Small antennas," *IEEE Trans. Antennas Propag.*, vol. AP-23, no. 4, pp. 462–469, Jul. 1975.
[52] I. Yamaura, "Mapping of microwave power transmitted through the human thorax," *Proc. IEEE*, vol. 67, no. 8, pp. 1170–1171, Aug. 1979.
[53] S. Salasche and G. Bernstein, *Surgical Anatomy of the Skin*. Stamford, CT: Appleton & Lange, 1988.
[54] G. J. Tortora and B. H. Derrickson, *Principles of Anatomy and Physiology*, 11 ed ed. New York: Wiley, 2006.
[55] P. Vodicka, J. K. Smetana, B. Dvoránková, T. Emerick, Y. Z. Xu, J. Ourednik, V. Ourednik, and J. Motlík, "The miniature pig as an animal model in biomedical research," *New York Acad. Sci.*, vol. 1049, pp. 161–171, 2005.
[56] T. P. Sullivan, W. H. Eaglstein, S. C. Davis, and P. Mertz, "The pig as a model for human wound healing," *Wound Repair Regen.*, vol. 9, pp. 66–76, 2001.
[57] C. R. D. Bass, K. A. Rafaels, R. S. Salzar, M. Carboni, R. W. Kent, M. D. Lloyd, S. Lucas, K. Meyerhoff, C. Planchak, A. Damon, and G. T. Bass, "Thoracic and lumbar spinal impact tolerance," *Accident Anal. Prevention*, vol. 40, pp. 487–495, 2008.
[58] *IEEE Std 802.15.4a—Part 15.4: Wireless Medium Access Control (MAC) and Physical Layer (PHY) Specifications for Low-Rate Wireless Personal Area Networks (WPANs)*, IEEE Standard 802.15.4a, 2007.
[59] A. Bensky, *Short-Range Wireless Communication: Fundamentals of RF System Design and Application*, 1st ed. London, U.K.: Newnes, 2000.
[60] R. N. Dean, J. Weller, M. J. M. J. Bozack, C. L. Rodekohr, B. Farrell, L. Jauniskis, J. Ting, D. J. Edell, and J. F. Hetke, "Realization of ultra fine pitch traces on LCP substrates," *IEEE Trans. Compon. Packag. Technol.*, vol. 31, no. 2, pp. 315–321, Jun. 2008.
[61] J. Weller, M. Bozack, B. Farrell, L. Jauniskis, J. Ting, D. Edell, and J. Hetke, "Micromachined LCP connectors for packaging MEMS devices in biological environments," *J. Microelectron. Electron. Packag.*, vol. 4, pp. 17–22, 2007.
[62] C. J. Lee, S. J. Oh, K. J. Song, and S. J. Kim, "Neural signal recording using microelectrode arrays fabricated on liquid crystal polymer material," *Mater. Sci. Eng.*, vol. 24, pp. 265–268, 2004.
[63] M. J. Chen, A. V. H. Pham, N. A. Evers, C. Kapusta, J. Iannotti, W. Kornrumpf, J. J. Maciel, and N. Karabudak, "Design and development of a package using LCP for RF/microwave MEMS switches," *IEEE Trans. Microw. Theory Tech.*, vol. 54, no. 11, pp. 4009–4015, Nov. 2006.
[64] "Standard test method for total mass loss and collected volatile condensable materials from outgassing in a vacuum environment," ASTM, West Conshohocken, PA, E595-93, 1999.
[65] H. Greenhouse, *Hermeticity of Electronic Packages*. New York: William Andrew, 2000.

Eric Y. Chow (S'07) received the B.S. degree in electrical and computer engineering from Cornell University, Ithaca, NY, in 2005, and the M.S.E.C.E and Ph.D. degrees from Purdue University, West Lafayette, IN, in 2007 and 2009, respectively.

Since 2002 he has held four internships with the Intel Corporation, where he has been with both the Digital and Analog Group in wireless communications. His interests include RF and low-power ASIC design, system integration of miniature implantable devices, and *in vivo* experimentation. His applications include treatment for epilepsy, spinal cord injury, glaucoma, and cardiac disease.

Yuehui Ouyang (S'03–M'05) was born in Nantong, China, in 1981. She received the B.S. degree in electrical engineering from the University of Science and Technology of China, Hefei, China, in 2003, and the M.S. and Ph.D. degrees in electrical engineering from Purdue University, West Lafayette, IN, in 2005 and 2008, respectively.

She is currently with the School of Electrical and Computer Engineering, Purdue University, as a Postdoctoral Research Associate. Her current research is focused on electro-textiles, wearable antennas, diversity design, wireless channel characterization, and integrated wireless bio-sensors.

Brooke Beier (S'09) received the B.S. degree in biomedical engineering from Purdue University, West Lafayette, IN, in 2008, and is currently working toward the Ph.D. degree in biomedical engineering at Purdue University.

Since 2007, she has performed research in the BCI Laboratory, Purdue University, as an undergraduate and graduate student. Her research has focused primarily on cardiac disease and spinal cord injury. Her interests include implantable biological device design and *in vivo* experimentation.

William J. Chappell (S'98–M'02) received the B.S.E.E., M.S.E.E., and Ph.D. degrees from The University of Michigan at Ann Arbor, in 1998, 2000, and 2002, respectively.

He is a member of the faculty with Purdue University, West Lafayette, IN, as an Assistant Professor. He is a member of the Birck Nanotechnology Center and the Center for Wireless Systems and Applications. His research focuses on silicon micromachining, polymer formation, and low-loss ceramics for high-frequency circuits and antennas. In addition, his research interests include rapid prototyping, free-form fabrication, and small-scale formation of electrically functioning ceramic and polymer passive components. He also oversees projects investigating RF design for wireless sensor networks, chemical sensors, and electrotextiles.

Dr. Chappell was the recipient of the 2004 Joel Spira Outstanding Educator Award. He has been designated as a Teacher for Tomorrow in his department.

Pedro. P. Irazoqui (S'94–M'03) received the B.Sc. and M.Sc. degrees in electrical engineering from the University of New Hampshire, Durham, in 1997 and 1999, respectively, and the Ph.D. degree in neuroengineering from the University of California at Los Angeles (UCLA), in 2003. His doctoral research concerned the design, manufacture, and packaging of implantable ICs for wireless neural recording.

Together with three partners, he helped found and was Vice President of IC development of Triangle Biosystems Inc., Research Triangle Park, NC. He is currently an Assistant Professor with the Weldon School of Biomedical Engineering, Purdue University, West Lafayette, IN, where his laboratory is involved with research into a modular approach to the design of biological implants in general and neural prosthetic devices in particular. These devices are being applied to the clinical treatment of physiological disorders, using miniature wireless implantable systems. The specific research and clinical applications explored in his laboratory include glaucoma, epilepsy, neural regeneration, and cardiac disease.

Dr. Irazoqui has been an associate editor of the IEEE TRANSACTIONS ON BIOMEDICAL ENGINEERING since late 2006. He was the recipient of the Best Teacher Award presented by the Weldon School of Biomedical Engineering (2006), the Early Career Award presented by the Wallace H. Coulter Foundation (2007), and the Marion B. Scott Excellence in Teaching Award presented by Tau Beta Pi (2008).